Nat. Hazards Earth Syst. Sci. Discuss., 2, 3711–3740, 2014
www.nat-hazards-earth-syst-sci-discuss.net/2/3711/2014/
doi:10.5194/nhessd-2-3711-2014

Natural Hazards and Earth System Sciences
Discussions
Open Access

Modeling inundation of seasonally flooded wetlands at McCarran Ranch on Truckee River, USA

X. Chen[1,2], L. Chen[1,3], J. Zhao[2], and Z. Yu[1]

[1]State Key Laboratory of Hydrology-Water Resources and Hydraulic Engineering, Hohai University, Nanjing, 210098, China
[2]College of Water Conservancy and Hydropower Engineering, Hohai University, Nanjing, 210098, China
[3]Division of Hydrologic Sciences, Desert Research Institute, Las Vegas, 89119, USA

Received: 1 April 2014 – Accepted: 4 May 2014 – Published: 27 May 2014

Correspondence to: L. Chen (lchen@dri.edu)

Published by Copernicus Publications on behalf of the European Geosciences Union.

Modeling inundation of seasonally flooded wetlands at McCarran Ranch on Truckee River, USA

X. Chen et al.

Abstract

This paper among the first presents the application and validation of a hydrodynamic model (Adaptive Hydraulics model, AdH) of the McCarran ranch. We use the AdH model with topographic data by combining the DEM data from USGS seamless server and the ESRI tin data from United States Army Corps of Engineers (USACE) to predict floodplain inundation for a river reach of ~10 km located at lower Truckee River in Nevada state. We tested the mesh independence, sensitivity of input parameters and time steps, and then compared the modeling results to the existing gauged data (both the discharge and water stage heights). Results show that the accuracy of prediction from AdH model can decline slightly at higher discharge and water levels. The modeling results are much sensitive to the roughness coefficient of main channel, suggesting the model calibration should give priority to the main channel roughness. The simulation results suggest that large flood events could lead to a significantly higher proportion of total flow that routed through the floodplains. During peak discharge, a river channel constriction diverted as much as 65 % of the river's 512.3 $m^3 s^{-1}$ discharge into the floodplain. During the overbank flow, the transboundary flux ratio is about 5–45 % of the total river discharge. Results also showed that both the relation of inundation area and volume between the discharge exhibit an apparent looped curve form.

1 Introduction

The pattern of flood inundation is of critical importance to the vegetation distribution in the floodplains in Lower Truckee River (Galat, 1990; McKenna et al., 1992). Temporal and spatial changes in flood inundation extent and water level have crucial roles in maintaining the sustainable organic material/nutrients exchanges between the main channel and floodplains, yet are critical for understanding hydrological and biogeochemical processes in aquatical ecosystems (Bayley, 1995; Antheunisse and Verhoeven, 2008; Pettit et al., 2011). The ability to model potential flood inundation and map actual extent of inundation, timing, and intensity under different flood levels is central to understanding the dynamics of ecological interactions in the main channel-floodplain system.

Roughly every ten years, the Truckee River generates a damaging flood. The 1997 inundation was a major event, putting downtown Reno under several feet of water and turning much of the Sparks industrial area into an inland sea. Although flooding is inevitable, progress is being made on flood control to make the area less prone to such risks (http://www.truckeeflood.us/). The use of satellite observations for evaluating the inundation extent and water level has been considered as an efficient way (Townsend and Walsh, 1998; Overton, 2005).However, currently available satellite observations of inundation extent and water level do not provide a solution as these are usually made using profiling altimeters with wide spacing between tracks (Birkett et al., 2002; Coe and Birkett, 2004), passive microwave instruments with good temporal but limited spatial resolution (Hamilton et al., 2002, 2004), or synthetic aperture radars with good spatial resolution but limited temporal coverage (Hess et al., 2003; Frappart et al., 2005). Whilst the regional significance of hydrology and biogeochemistry process in Truckee River floodplains is undisputed, inundation analysis needs a higher accuracy at a much finer spatial and temporal resolutions.

As an increase in accuracy and reliability of flow and inundation predictions is desirable for better decisions concerning land use and water management, the development and improvement of methods for high-resolution hydrologic modeling has been increasingly committed (Neal et al., 2012). Significant advances in flood inundation modeling have been achieved in the last decade through the use of a new generation of two-dimensional (2-D) hydraulic numerical models (Leopardi et al., 2002; Hunter et al., 2007; Neal et al., 2011). These offer the potential to predict the local pattern and timing of flood depth and velocity, enabling informed flood risk zoning and improved emergency planning. This paper demonstrates the application of a 2-D Adaptive Hydraulics model (AdH) with fine resolution, and the validation of the ability of such a code to simulate flood dynamics on a topographically complex floodplain. Also, the characterization of flow exchanges in channel-floodplains system and the inundation feature of the McCarran ranch were studied based on the modeling results.

2 Modeling approach

2.1 Governing equations and model settings

The 2-D shallow water module of AdH solves the 2-D nonlinear shallow water equations. These equations have proven successful in describing water surface and velocity fields in surface water modeling and accepted by many authors as it appears that most studies use 2-D models (Abderrezzak et al., 2009; Mignot et al., 2006; Bates et al., 2010; deAlmeida et al., 2012). The equations are derived with the assumption that the vertical velocity component is negligible. Neglecting shear stress and fluid pressure at the free surface, the 2-D shallow water equations as implemented within AdH are written as:

$$\frac{\partial Q}{\partial t} + \frac{\partial F_x}{\partial x} + \frac{\partial F_y}{\partial y} + H = 0 \tag{1}$$

where,

$$Q = \begin{Bmatrix} h \\ uh \\ vh \end{Bmatrix} \tag{2}$$

$$F_x = \begin{Bmatrix} uh \\ u^2 h + \frac{1}{2} g h^2 - h \frac{\sigma_{xx}}{\rho} \\ uvh - h \frac{\sigma_{yx}}{\rho} \end{Bmatrix} \tag{3}$$

NHESSD
2, 3711–3740, 2014

$$F_y = \begin{Bmatrix} vh \\ uvh - h\frac{\sigma_{yx}}{\rho} \\ v^2h + \frac{1}{2}gh^2 - h\frac{\sigma_{yy}}{\rho} \end{Bmatrix} \quad (4)$$

$$H = \begin{Bmatrix} 0 \\ gh\frac{\partial z_b}{\partial x} + n^2 g\frac{u\sqrt{u^2+v^2}}{h^{1/3}} \\ gh\frac{\partial z_b}{\partial y} + n^2 g\frac{v\sqrt{u^2+v^2}}{h^{1/3}} \end{Bmatrix} \quad (5)$$

The Reynolds stresses are determined using the Boussinesq approach to the gradient in the mean currents,

$$\sigma_{xx} = 2\rho v_t \frac{\partial u}{\partial x} \quad (6)$$

$$\sigma_{yy} = 2\rho v_t \frac{\partial v}{\partial y} \quad (7)$$

$$\sigma_{xy} = \sigma_{yx} = 2\rho v_t \left(\frac{\partial u}{\partial y} + \frac{\partial v}{\partial x}\right) \quad (8)$$

where, h is flow depth, u and v are velocities in x and y directions, g is gravitational acceleration, ρ is flow density, σ_{xx}, σ_{yy}, σ_{xy} and σ_{yx} are shear stresses, where the first subscript indicates the direction, and the second indicates the face on which the stress acts, are due to turbulence. z_b is the river bed elevation and n is Manning's friction coefficient. v_t is the kinematic eddy viscosity, which varies spatially where turbulence closure is achieved through the algebraic eddy viscosity formulation described by Rodi (1993).

The critical input data is the Digital Elevation Model (DEM) of sufficient resolution and vertical accuracy to capture floodplain topographic features relevant to flow development at the scale of interest and channel bathymetric information detailing the longitudinal slope. The channel bathymetry was captured using the ESRI tin data obtained from

NHESSD
2, 3711–3740, 2014

United States Army Corps of Engineers (USACE). The floodplain topology data was created from the 30 × 30 m United States Geological Survey (USGS) Digital Elevation Model (DEM) obtained from the USGS seamless server (http://seamless.usgs.gov/) and it was integrated into the ESRI tin data obtained from USACE. The DEM is necessary for delineating the study area and assigning elevation for individual grid cells (Bates and De Roo, 2000). The modeling area is depicted in Fig. 1. The AdH model was developed for the river reach of approximately 10 km in length.

The other group of input parameters was the surface roughness. These parameters are generally associated with the land use information. The land use data was obtained from the webGIS website (http://www.webgis.com). It was used to determine the surface roughness with referenced data obtained from the tabular values in Chow (1988). Fine tuning of the roughness value was later on carried out in model calibration. The land use pattern within the AdH model boundary is shown in Fig. 2a. Also, the estimated eddy viscosity function with a coefficient value of 0.5 was used for this study. As the element wetting and drying limits could cause model instabilities that require an elaborate adjustment (Gambucci, 2009; Karadogan and Willson, 2010). We set the values at 0.15 m for both the wetting and drying limits. Results of testing models showed that changes in these values have very little impact on the hydrodynamic results.

There is only one gauging station (USGS 10350340) in the study reach. This gauge is located at the lower part of the study area (Fig. 1) and started operation from June, 1997. Data from this station were used for model validation. The nearest gauging station (USGS 10350000) is upstream to the study reach. It has record since January, 1995. Data from this station were used as inputs in a HEC-RAS simulation, and the output hydrograph was used as an upstream boundary condition of the study reach. Also, for flood events that happened before June, 1997, the outputs of HEC-RAS on the USGS gauging profile were used for validation. The river stage values also obtained from HEC-RAS simulation results was used for downstream boundary condition. The observed river flow was obtained from USGS NWIS (http://waterdata.usgs.gov/nwis/sw). It was used to compare the modeled flow with the observation.

2.2 Mesh dependence

The adaptive numerical mesh within the AdH model can improve model accuracy without sacrificing efficiency. Before applying the adaptive mesh approach, a base level mesh needs to be generated first. The mesh was created in software Surface Modeling System (SMS) which can be used as a pre- and post-processing graphic user interface for AdH. Following mesh generation, the bathymetric data of the stream was interpolated onto the mesh nodes. Triangular elements were used to discrete the domain is shown in Fig. 2b. Special care was taken to generate a fine mesh in the vicinity of the main channel. Since the simulation results depend on the mesh resolution and quality, several mesh resolutions were adopted for mesh dependence study (Table 1). To compare with the observation, the simulated velocity and water depth on the profile where the USGS gauging station located were extracted. Figure 3a and b shows the velocity and water depth corresponding to different element number on the peak flow stage for a high discharge flood happened in the early January in 1997. The time step (Δt) was set to 1 s. Results show that simulation with mesh density M2 and above were mesh independent.

2.3 Time step sensitivity study

AdH is an implicit code and therefore, the time step size is not stability limited for the linear problem, however, nonlinear instability will occur if the time step is too large (Tate et al., 2009). Choosing a proper initial time step could reduce the turnaround time on time-critical simulations. Three different initial time step sizes were chosen for investigating the initial time step dependence (see Table 2). Same as the mesh dependence analysis, the depth and velocity value along the gauging profile at the peak flow stage in the early January, 1997 were used for comparison. As showing in

Fig. 4, both the velocity and depth along the gauging profile are plotted for particular time levels. From Fig. 4 it can be note that the initial time step sizes of 30 s is good enough to capture the physical properties of floods modeling results.

3 Results and discussion

3.1 Model test

We have established a finite element model for the chosen study area. The number of mesh grid is described in the case M2, and the initial time step size was set to 30 s. For a higher accuracy, the mesh adaptive technology was used for mesh refinement to get better results. Generally, the number of FEM nodes during the interaction ranged from 6307 to 7911. The devastating flood in early 1997 was chosen as a typical flood for model calibrations and validations. Due to the large inundation area during this flood event, it is more appropriate to analyze the impacts of floodplain roughness on the flood propagation. Roughness coefficient of main channel and floodplains were set separately for model calibration. In order to examine the model response to roughness coefficient, we ran a matrix of 25 simulations with values of n_c (Roughness coefficient for the main channel) varying from 0.036 to 0.041 in 0.001 increments and n_f (Roughness coefficient for the floodplains) varying from 0.044 to 0.05 in 0.002 increments. Outputs from the model was compared with the observed values available at the gauging station near the outlet of the river reach. Here we calculated the time series discharge across the gauging profile based on the velocity magnitude and water depth value along the profile line (showing in Fig. 1). The Accuracy for all simulations was then calculated using the Nash–Sutcliffe efficiency criteria (Nash and Sutcliffe,1970),

E_f:

$$E_f = 1 - \frac{\sum^n \left(\hat{Y}_i - Y_i\right)^2}{\sum^n \left(Y_i - \overline{Y}\right)^2} \tag{9}$$

in which $\hat{Y}_i$ and Y_i are predicted and measured values of the criterion dependent variable Y, respectively; $\overline{Y}$ is the mean of the measured values of Y; and n is the sample size. E_f ranges between $-\infty$ (where the observed mean is a better predictor than the model) to 1 (where observed and predicted values are identical). The Nash–Sutcliffe coefficient has been considered as a goodness of fit index to systemically assess effectiveness of hydrological models (Krause et al., 2005; McCuen et al.,2006). By calculating the E_f value for the 25 scenarios, it is found that the index value ranged from 0.770 with the lowest main channel roughness ($n_c = 0.036$) to 0.937 with the roughness of main channel equals to 0.039. The change of roughness of floodplains makes less difference in the Nash–Sutcliffe index (for example, the E_f value ranges from 0.924 to 0.937 with the n_f gradually varying from 0.044 to 0.05, while keeping n_c with a constant value to 0.039), suggesting that the modeled flood discharge is much more sensitive to the main channel friction than the floodplain friction. Base on this understanding on the roughness impacts, the calibrated roughness coefficient of main channel was set to 0.039, while the roughness coefficients for other land use types are set to 0.048 (grass land), 0.05 (crop land), 0.011 (high way) and 0.05 (strip mines), respectively. The model was validated by using the adjusted roughness coefficients for the flood occurred in early January, 1997. The corresponded E_f is equal to 0.933, showing a good goodness-of-fit.

The calibrated model is further applied to simulate different flood events in order to examine the applicability and accuracy of simulation model in details. As shown in Fig. 5, we chose six other flood events for testing cases in addition to the flood event in early 1997. These cases were sorted with index numbers according to the magnitude of peak flow. Comparison to the gauging station data (both the discharge and water level) for the 7 testing cases is shown in Figs. 6 and 7. The scatter plot comparison for all data is shown at the lower right corner in each figure. The commonly used accuracy measure RMSE (Root Mean Square Error) is calculated for each testing cases (shown in sub-figures in both Fig. 6 and Fig. 7). The overall RMSE for all testing cases to the discharge comparison throughout the simulation was $5.83\,\mathrm{m^3\,s^{-1}}$. This was reduced to $3.06\,\mathrm{m^3\,s^{-1}}$ for discharge less than $100\,\mathrm{m^3\,s^{-1}}$ and increased to $6.94\,\mathrm{m^3\,s^{-1}}$ for discharge higher than $100\,\mathrm{m^3\,s^{-1}}$. The model predicted the low flow much better (RMSE ranges 0.90 to $1.70\,\mathrm{m^3\,s^{-1}}$ for testing cases ① ∼ ③) and the model performance reduced during high flow (RMSE ranges 3.13 to $14.65\,\mathrm{m^3\,s^{-1}}$ for testing cases ④ ∼ ⑦). Similar in Fig. 6, the overall RMSE of water depth for all testing cases throughout the simulation was 0.12 m. The accuracy of model predictions was higher for lower water levels (RMSE was 0.07 m for water depth less than 3 m and enlarged to 0.13 m for water depth higher than 3 m). For the relatively lower flow cases (testing cases ① ∼ ③), the RMSE ranged from 0.009 to 0.015 m, showing a good accuracy of predictions at low water. The RMSE for relevant higher flow (testing cases ④ ∼ ⑦) ranged from 0.05 to 0.22 m, showing a less accuracy of predictions at high water levels.One main cause of the error for water level is likely due to the resolution of the topographic data. The vertical elevation of finite element mesh nodes were interpolated from the coarse DEM (30 m) and ESRI tin data, errors existed in the terrain data of study reach. Another source of the error may come from the vertical accuracy of the elevation/bathymetry data. Also, the zoning and spatial properties for each element of the whole modeling domain were primarily based on the land use data and led to temporally constant parameters, which may not reflect the real conditions. Flow roughness could be affected by this reason. Although the roughness coefficients had been calibrated for the modeling period, they probably cannot accurately represent the real friction factor of each land use type at all time (e.g. vegetation property would change seasonally). Also, treating the roughness coefficients as constant values independent of flow depth in AdH modeling would result in errors. In reality, flow roughness can change with the water levels over the floodplain (Domeneghetti et al., 2012). Moramarco and Singh (2010) evaluated the trend of Manning's coefficient for two river sites along the Tiber River and they highlighted that the *n* value decreases with increasing flow depth (and hence increasing discharge), showing an asymptotical behavior for high water levels. Furthermore, the neglecting of both the evaporation and infiltration would be another error factor. Despite modeling errors appearing in high flows, the model provides a much detailed view of floodplain hydraulics that can enhance our understanding of water interactions between main channel and floodplains.

3.2 Characterization of exchanges between main channel and floodplains

We assessed the hydrological connectivity between the main channel and its floodplains with two approaches. First, we examined the spatial variation in the flux distribution at 12 different locations (marked in Fig. 1) along the focused river reach. We calculated the averaged longitudinal flux passing through the floodplains (Q_{fp}).The proportion of total flow that routed through the floodplains (α_{fp}) was then obtained by dividing Q_{fp} with total discharge. Second, we examined the transboundary flux of both river banks along the focused reach, which is defined as the flow flux penetrating the boundary between the main channel and floodplains along a selected reach. The transboundary flux ratio (β_{ex}) was then calculated by dividing the total transboundary flux with inflow discharge.

Quantifying the flux distribution is generally considered a good way to identify the river–floodplain exchange flux and connectivity (Thomaz et al., 2007; Heiler et al., 1995). Previous studies have shown that the lateral exchange can be considerably complicated and strongly depends on channel morphology, and both the magnitudes and direction of lateral flux are spatial-related variables. Such exchange cannot be simply described by a single flow quantity and needs to be examined in different aspect. The proportion of total flow routing through the floodplains (α_{fp}) is considered a useful indicator for flux distribution. Its magnitude and spatiotemporal change can disclose some details of the hydraulic role of the floodplains and the interaction between the

NHESSD
2, 3711–3740, 2014

main channel and the floodplains. For McCarran ranch, this ratio is calculated at each flux sampling location for 7 different discharge, carrying out 84 calculations in total. The results are plotted in Fig. 8a. As shown, the error bars represent the spatial heterogeneity of the flux distribution in the river–floodplain system, and the mean values represent the averaged flux proportion that routing through the overall floodplains of the focused reach. The distribution of flux could have been caused by the flow pattern of the meandering channel. For example, since transects No. 6 and No. 11 (Fig. 1) have stronger meandering feature comparing to other transects (e.g., transect No.2 locates at a much straighter reach), the flux on the adjacent floodplains at these transects can be $3.2 \sim 5.3$ times of a straight reach while the peak discharge is $248.4\,\mathrm{m^3\,s^{-1}}$, with the rising of flux rate, the clout of meandering course is waning. The factor reduces to $2.3 \sim 4.1$ when the discharge is as high as $521.3\,\mathrm{m^3\,s^{-1}}$. Also, the lateral slope in terrain could be another cause to the flux distribution in main channel-floodplain system. Due to the relatively higher slope of hill slopes at transect No.1, the α_{fp} always has the lowest value comparing to other transects.

The ratio α_{fp} increases with rising flow discharge. As shown in Fig. 8a, the relation between the mean proportion and discharge can be fitted with a power-law function (a straight line in logarithmic scales with a slope of 1.5) with high goodness-of-fit ($R^2 = 0.984$). Despite this power law relationship for flood water exchange ratio was obtained from a specified study reach of Truckee River, and may not necessarily be applicable to other sites, it reveals the fact that the floods have a significant impact on the flux exchange in a river–floodplain system, and this would consequently affect the nutrients and organic matters transport.

The mean value of α_{fp} for McCarran ranch from year 1995 to 2000 is calculated by applying the power law function, shown in Fig. 8b. Similar to the discharge trend, α_{fp} is seasonally fluctuated according to the floods. Generally, the proportion of flux routing through floodplains at McCarran ranch is less than 5 % during base flow, and it can reach to 15–30 % during small flood events. During extreme high floods, this ratio can be as high as 65 %, representing a much high proportion of total flow that routed through the floodplains. Our results are compatible to other results reported in literature. Similar research results have been reported in other river system studies. Richey et al. (1989) used Muskingum routing of main channel flow and simple floodplain representation to estimate the flow volume exchanges in river–floodplain systems at Itapena of Amazon River, their research results showed that the ratio of exchanged flux was approximately 30 %. Wilson et al. (2007) updated this result based on 2-demensional modeling and found the ratio to be at least 40 % between Itapeua and Manaus on Amazon River. Zurbrügg et al. (2012) have estimated the river–floodplain exchange in Kafue Flats through high resolution measurements of discharge and tracers, and found this exchange ratio to be as much as 80 % during peak discharge. This river–floodplain exchange flow could have a strong impact on river quality, and resulting in seasonally recurring sharp changes in dissolved oxygen levels or other quality objectives (Zurbrügg et al., 2012, 2013).

A more direct look of the river–floodplain exchange is the transboundary flux, which is defined as the flow discharge penetrating the boundary between the main channel and floodplains. The transboundary flux vs. river discharge of two particular flood events was plotted in Fig. 9. The fluxes were used to determine the quantity of floodwater from the main channel to the floodplains. As shown in Fig. 9, the maximum transboundary flux occurred before the peak flow for each flood event. Generally, the transboundary flux ratio is approximately from 0.05 to 0.45, and the corresponded flux is 8 $m^3 s^{-1}$ to 70 $m^3 s^{-1}$. The variation of transboundary flux is mainly controlled by the magnitude of flood discharge, e.g. when the discharge is increased from 270 $m^3 s^{-1}$ to 550 $m^3 s^{-1}$, the total tranboundary flux is increased from 30 $m^3 s^{-1}$ to 65 $m^3 s^{-1}$ accordingly. The opposite flow across the river boundary at rising stage and receding stage leads to the loop curve relation between transbounday flux and discharge.

3.3 Flood inundation analysis

The prediction of flood inundation is crucial for risk control and water resources management. Both the inundation area and volume were numerically calculated from the

AdH modeling results. A Matlab code was developed for the inundation area and volume calculation based on water depth values on mesh nodes (outputs of AdH) and the finite element mesh information (inputs of AdH). The extreme flood event occurred in early January in 1997 was set as an example for inundation analysis. The inundated area and volume were calculated at different discharges that chosen from the flood rising stage, peak flow stage and recession stage. Figure 10 shows the scatter plots of inundated area and inundated volume. The maximum inundated area and volume can be as high as 1.3 km^2 and 3.95×10^6 m^3, respectively. More interestingly, we found that both the inundated area–discharge relation and inundated volume–discharge relation show a looped curve pattern. These looped curves indicate that the same flow discharge at different stages of a flood produced different inundated areas or volumes. This is similar to the looped rating curve for stage–discharge relation during flood events. Based on literature survey, the looped curve pattern of the inundated area or volume–discharge relation has not been reported yet in the previous studies. This result has a great value in practice for flood risk mitigation in improving the flood disaster assessment and risk estimation. Furthermore, the inundated area–discharge relation describes an areal result rather than at a station, i.e., an upscaled result of the point-scale stage–discharge relation. It shows that such hysteresis effect can appear not only at local scales, but also at large spatial scales. This result can help us further understand the flood regime and related biogeochemical processes.

4 Conclusions

The use of the hydrodynamic model (AdH) is an effective method for delineating flood inundation in areas of subtle topographic relief. This model was applied for modeling the seasonally flood river at McCarran ranch on Truckee River with a much finer mesh grids. The model was calibrated with gauge data and the validated model performed well in representing the flood hydrographs of various magnitudes. Although the accuracy of prediction declined slightly at higher discharge and water stage, the raw output

NHESSD
2, 3711–3740, 2014

of depth and velocity magnitudes from a 2-D form of AdH appears adequate to produce reasonable results.

Results show that the proportion of flow that routed through floodplains is much higher during extreme flood events. Since the river–floodplain exchange plays a crucial role in maintaining ecosystem, estimating the exchange ratio through a modeling approach could be useful for river restoration and river landscape design, or even be used as a global index for river ecological assessment. However, field measurements are still recommended for further verification of AdH modeling results.

The inundation area (or volume)–discharge relation at McCarran Ranch on Truckee River was found to be a looped curve pattern, showing hysteresis of flood inundation exists in large spatial scales. Despite this result was obtained from a specific river reach, it will be potentially useful for flood risk assessment and water resources management of other river–floodplain systems, especially for rivers with considerably more floodplain areas.

Acknowledgements. The work was funded by US Army Corps of Engineering (W912HZ-08-2-0021) and partially funded by the National Natural Science Foundation of China (51279045). Thanks to Eleeja Shrestha for assistance with data collection.

References

Abderrezzak, K. E. K., Paquier, A., and Mignot, E.: Modelling flash flood propagation in urban areas using a two-dimensional numerical model, Nat. Hazards, 50, 433–460, 2009.

Antheunisse, A. M. and Verhoeven, J. T.: Short-term responses of soil nutrient dynamics and herbaceous riverine plant communities to summer inundation, Wetlands, 28, 232–244, 2008.

Bates, P. D. and De Roo, A. P. J.: A simple raster-based model for flood inundation simulation, J. Hydrol., 236, 54–77, 2000.

Bates, P. D., Horritt, M. S., and Fewtrell, T. J.: A simple inertial formulation of the shallow water equations for efficient two-dimensional flood inundation modelling, J. Hydrol., 387, 33–45, 2010.

NHESSD

2, 3711–3740, 2014

Bayley, P. B.: Understanding large river: floodplain ecosystems, Bioscience, 45, 153–158, 1995.
Birkett, C. M., Mertes, L. A. K., Dunne, T., Costa, M. H., and Jasinski, M. J.: Surface water dynamics in the Amazon Basin: application of satellite radar altimetry, J. Geophys. Res., 107, 8059, doi:10.1029/2001JD000609, 2002.
Chow, V., Maidment, D. R., and Mays, L. W.: Applied Hydrology, Tata McGraw-Hill Education, 1988.
Coe, M. T. and Birkett, C. M.: Calculation of river discharge and prediction of lake height from satellite radar altimetry: example for the Lake Chad basin, Water Resour. Res., 40, W10205, doi:10.1029/2003WR002543, 2004.
de Almeida, G. A. M., Bates, P., Freer, J. E., and Souvignet, M.: Improving the stability of a simple formulation of the shallow water equations for 2-D flood modeling, Water Resour. Res., 48, W05528, doi:10.1029/2011WR011570, 2012.
Domeneghetti, A., Castellarin, A., and Brath, A.: Assessing rating-curve uncertainty and its effects on hydraulic model calibration, Hydrol. Earth Syst. Sci., 16, 1191–1202, doi:10.5194/hess-16-1191-2012, 2012.
Frappart, F., Seyler, F., Martinez, J. M., León, J. G., and Cazenave, A.: Floodplain water storage in the Negro River basin estimated from microwave remote sensing of inundation area and water levels, Remote Sens. Environ., 99, 387–399, 2005.
Galat, D. L.: Seasonal and long-term trends in Truckee River nutrient concentrations and loadings to Pyramid Lake, Nevada: a terminal saline lake, Water Res., 24, 1031–1040, 1990.
Gambucci, T.: ADH = fast and stable 2D finite element model, in: Proceedings of World Environmental and Water Resources Congress, 2816–2822, 2009.
Hamilton, S. K., Sippel, S. J., and Melack, J. M.: Comparison of inundation patterns among major South American floodplains, J. Geophys. Res., 107, doi:10.1029/2000JD000306, 2002.
Hamilton, S. K., Sippel, S. J., and Melack, J. M.: Seasonal inundation patterns in two large savanna floodplains of South America: the Llanos de Moxos (Bolivia) and the Llanos del Orinoco (Venezuela and Colombia), Hydrol. Process., 18, 2103–2116, doi:10.1002/hyp.5559, 2004.
Heiler, G., Hein, T., Schiemer, F., and Bornette, G.: Hydrological connectivity and flood pulses as the central aspects for the integrity of a river–floodplain system, Regul. River., 11, 351–361, 1995.

Discussion Paper | Discussion Paper | Discussion Paper | Discussion Paper |

Hess, L. L., Melack, J. M., Novo, E. M., Barbosa, C. C., and Gastil, M.: Dual-season mapping of wetland inundation and vegetation for the central Amazon basin, Remote Sens. Environ., 87, 404–428, 2003.
Hunter, N. M., Bates, P. D., Horritt, M. S., and Wilson, M. D.: Simple spatially-distributed models for predicting flood inundation: a review, Geomorphology, 90, 208–225, 2007.
Karadogan, E. and Willson, C. S.: Simulating the impact of medium and large diversions on the hydrodynamics in the lower Mississippi River Delta, in: River Flow 2010 Proceedings of the International Conference on Fluvial Hydraulics, edited by: Dittrich, Koll, Aberle and Geisenhainer, 1581–1588, 2010.
Krause, P., Boyle, D. P., and Bäse, F.: Comparison of different efficiency criteria for hydrological model assessment, Adv. Geosci., 5, 89–97, doi:10.5194/adgeo-5-89-2005, 2005.
Leopardi, A., Oliveri, E., and Greco, M.: Two-dimensional modeling of floods to map risk-prone areas, J. Water Res. Pl.-ASCE, 128, 168–178, 2002.
McCuen, R. H., Knight, Z., and Cutter, A. G.: Evaluation of the Nash–Sutcliffe efficiency index, J. Hydrol. Eng., 11, 597–602, 2006.
McKenna, S. A., Ingraham, N. L., Jacobson, R. L., and Cochran, G. F.: A stable isotope study of bank storage mechanisms in the Truckee River basin, J. Hydrol., 134, 203–219, 1992.
Mignot, E., Paquier, A., and Haider, S.: Modeling floods in a dense urban area using 2D shallow water equations, J. Hydrol., 327, 186–199, 2006.
Moramarco, T. and Singh, V. P.: Formulation of the entropy parameter based on hydraulic and geometric characteristics of river cross sections, J. Hydrol. Eng., 15, 852–858, 2010.
Nash, J. and Sutcliffe, J. V.: River flow forecasting through conceptual models part I – A discussion of principles, J. Hydrol., 10, 282–290, 1970.
Neal, J., Schumann, G., Fewtrell, T., Budimir, M., Bates, P., and Mason, D.: Evaluating a new LISFLOOD-FP formulation with data from the summer 2007 floods in Tewkesbury, UK, Journal of Flood Risk Management, 4, 88–95, 2011.
Neal, J., Villanueva, I., Wright, N., Willis, T., Fewtrell, T., and Bates, P.: How much physical complexity is needed to model flood inundation?, Hydrol. Process., 26, 2264–2282, 2012.
Overton, I. C.: Modelling floodplain inundation on a regulated river: integrating GIS, remote sensing and hydrological models, River Res. Appl., 21, 991–1001, 2005.
Pettit, N. E., Bayliss, P., Davies, P. M., Hamilton, S. K., Warfe, D. M., Bunn, S. E., and Douglas, M. M.: Seasonal contrasts in carbon resources and ecological processes on a tropical floodplain, Freshwater Biol., 56, 1047–1064, 2011.

Richey, J. E., Mertes, L. A. K., Dunne, T., Victoria, R. L., Forsberg, B. R., Tancredi, A. C. N. S., and Oliveira, E.: Source and routing of the Amazon River flood wave, Global Biogeochem. Cy., 3, 191–204, 1989.
Rodi, W.: Turbulance Models and their Application in Hydraulics: a State-of-the-Art Review, Taylor and Francis Group, Balkema, Leiden, 1993.
Tate, J., McAlpin, T. O., and Savant, G.: Modeling Dam/Levee Breach Scenarios Using the Adaptive Hydraulics Code, in: 2009 AWRA Annual Water Resources Conference, Seattle, Washington, 2009.
Thomaz, S. M., Bini, L. M., and Bozelli, R. L.: Floods increase similarity among aquatic habitats in river–floodplain systems, Hydrobiologia, 579, 1–13, 2007.
Townsend, P. A. and Walsh, S. J.: Modeling floodplain inundation using an integrated GIS with radar and optical remote sensing, Geomorphology, 21, 295–312, 1998.
Wilson, M., Bates, P., Alsdorf, D., Forsberg, B., Horritt, M., Melack, J., Frappart, F., and Famiglietti, J.: Modeling large-scale inundation of Amazonian seasonally flooded wetlands, Geophys. Res. Lett., 34, L15404, doi:10.1029/2007GL030156, 2007.
Zurbrügg, R., Wamulume, J., Kamanga, R., Wehrli, B., and Senn, D. B.: River-floodplain exchange and its effects on the fluvial oxygen regime in a large tropical river system (Kafue Flats, Zambia), J. Geophys. Res., 117, G03008, doi:10.1029/2011JG001853, 2012.
Zurbrügg, R., Suter, S., Lehmann, M. F., Wehrli, B., and Senn, D. B.: Organic carbon and nitrogen export from a tropical dam-impacted floodplain system, Biogeosciences, 10, 23–38, doi:10.5194/bg-10-23-2013, 2013.

NHESSD
2, 3711–3740, 2014

Modeling inundation of seasonally flooded wetlands at McCarran Ranch on Truckee River, USA

X. Chen et al.

Table 1. Scenarios of mesh dependence testing.

Mesh testing	No. of elements
M1	4911
M2	6307
M3	10 306

NHESSD

2, 3711–3740, 2014

Table 2. Scenarios of time sensitivity study.

Time sensitivity testing	Time step(s)
Δt_1	1
Δt_2	10
Δt_3	30

NHESSD
2, 3711–3740, 2014

Title Page
Abstract Introduction
Conclusions References
Tables Figures
Back Close
Full Screen / Esc
Printer-friendly Version
Interactive Discussion

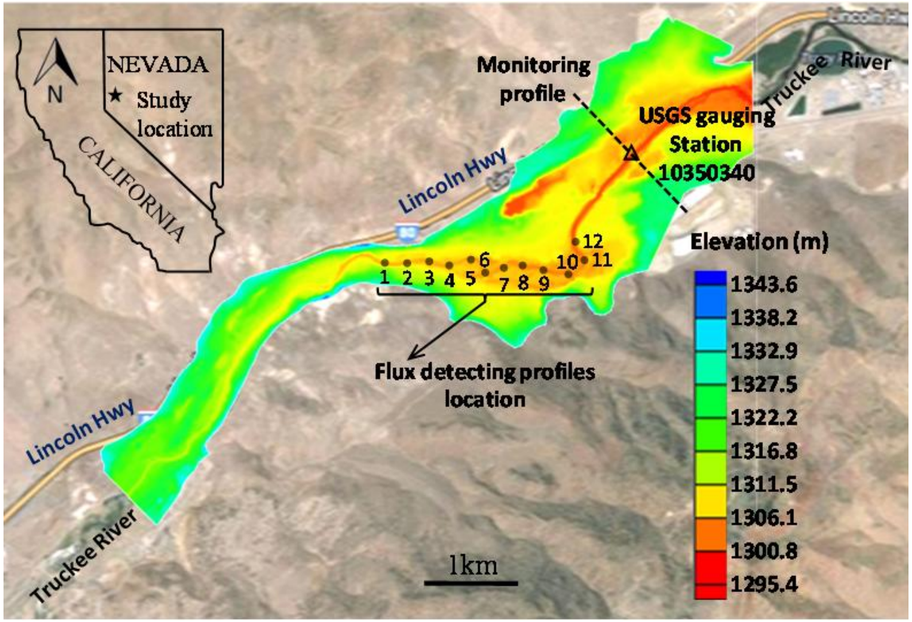

Figure 1. Study location and the elevation of focused area.

NHESSD
2, 3711–3740, 2014

Modeling inundation of seasonally flooded wetlands at McCarran Ranch on Truckee River, USA

X. Chen et al.

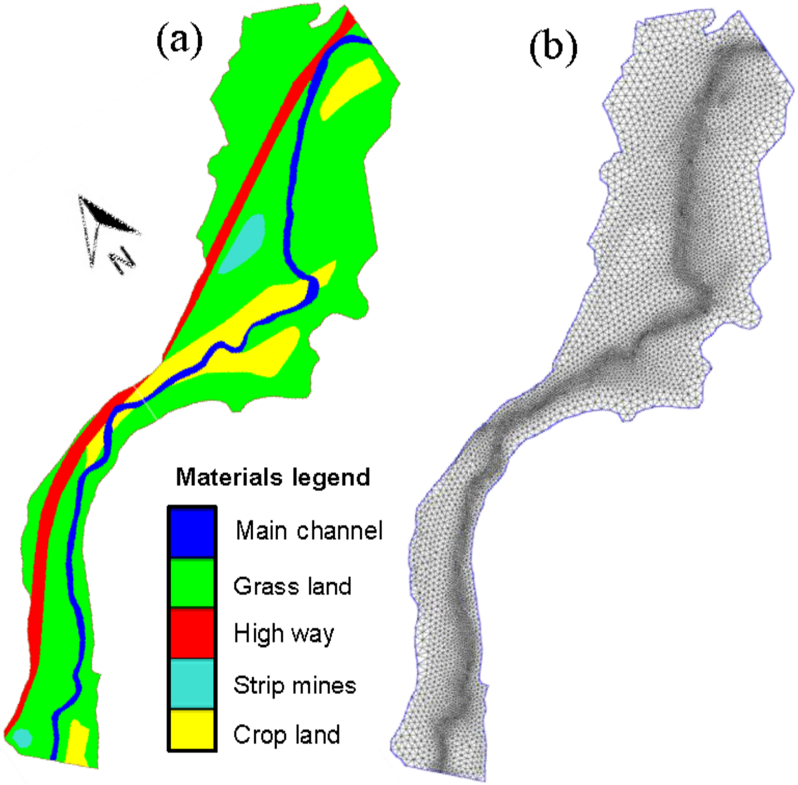

Figure 2. The landuse information **(a)** and finite element mesh **(b)** of study area.

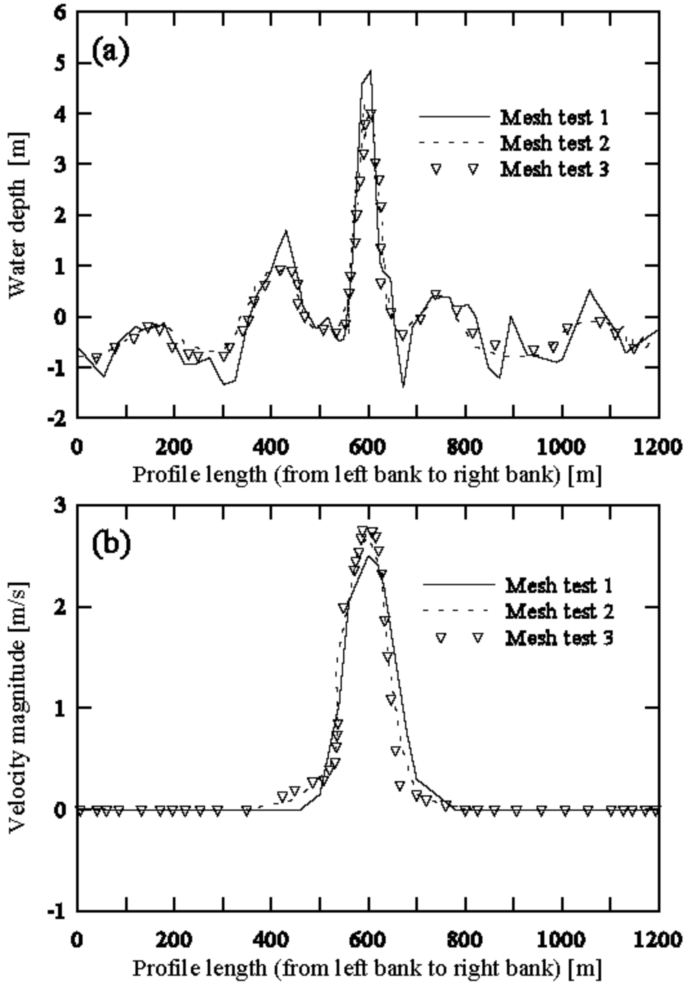

Figure 3. Results of mesh dependence testing.

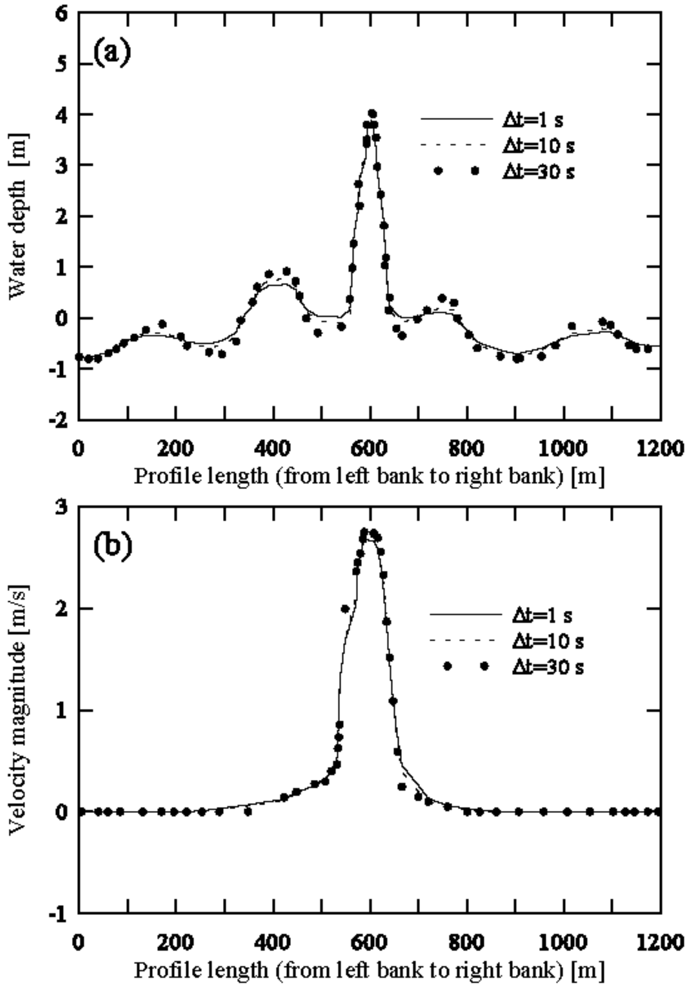

Figure 4. Results of time sensitivity study.

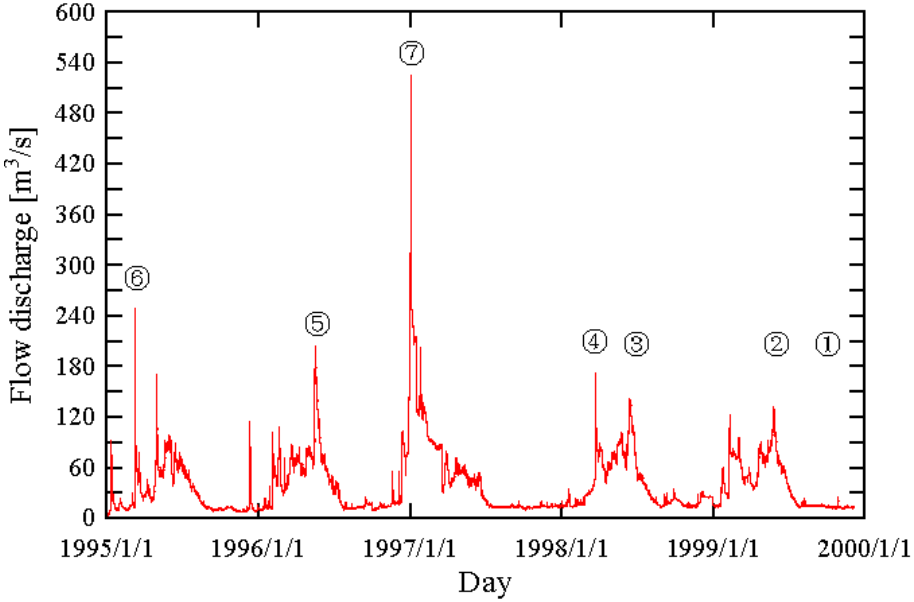

Figure 5. Scenarios of flood events, of which, case ⑥ and case ⑦ are representing the 10 yr and 50 yr flood events, respectively.

NHESSD
2, 3711–3740, 2014

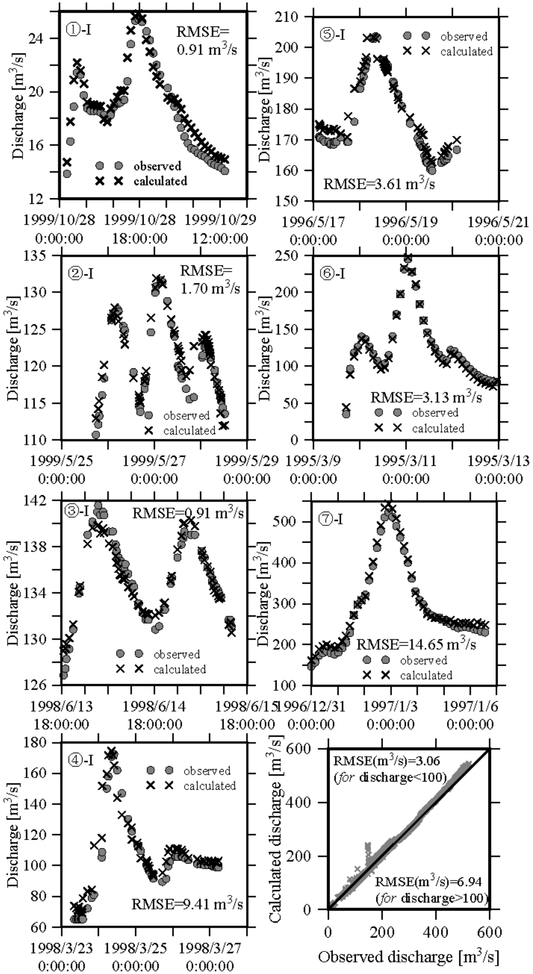

Figure 6. Comparison of calculated discharge and observed discharge.

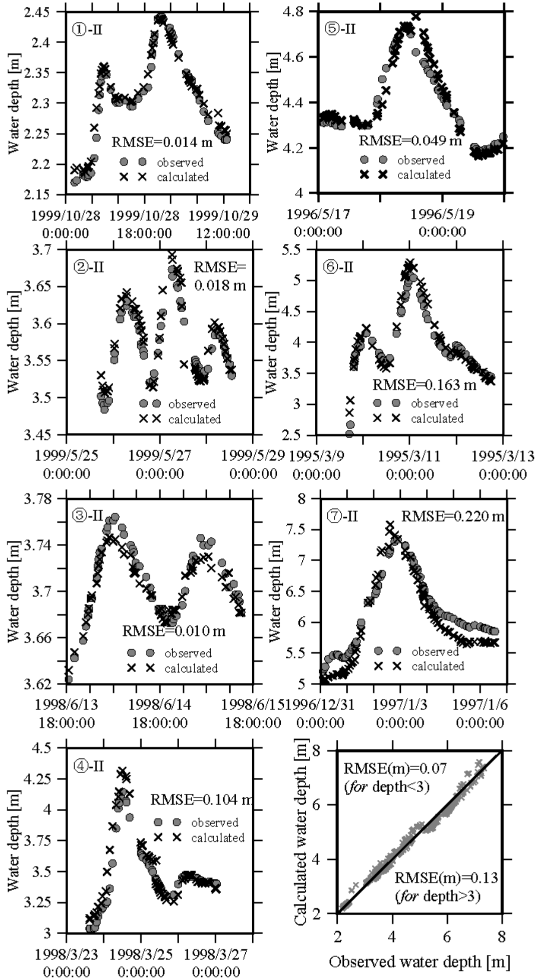

Figure 7. Comparison of calculated water depth and observed water depth.

NHESSD
2, 3711–3740, 2014

Modeling inundation of seasonally flooded wetlands at McCarran Ranch on Truckee River, USA

X. Chen et al.

Title Page
Abstract | Introduction
Conclusions | References
Tables | Figures
◀| |▶
◀ ▶
Back | Close
Full Screen / Esc
Printer-friendly Version
Interactive Discussion

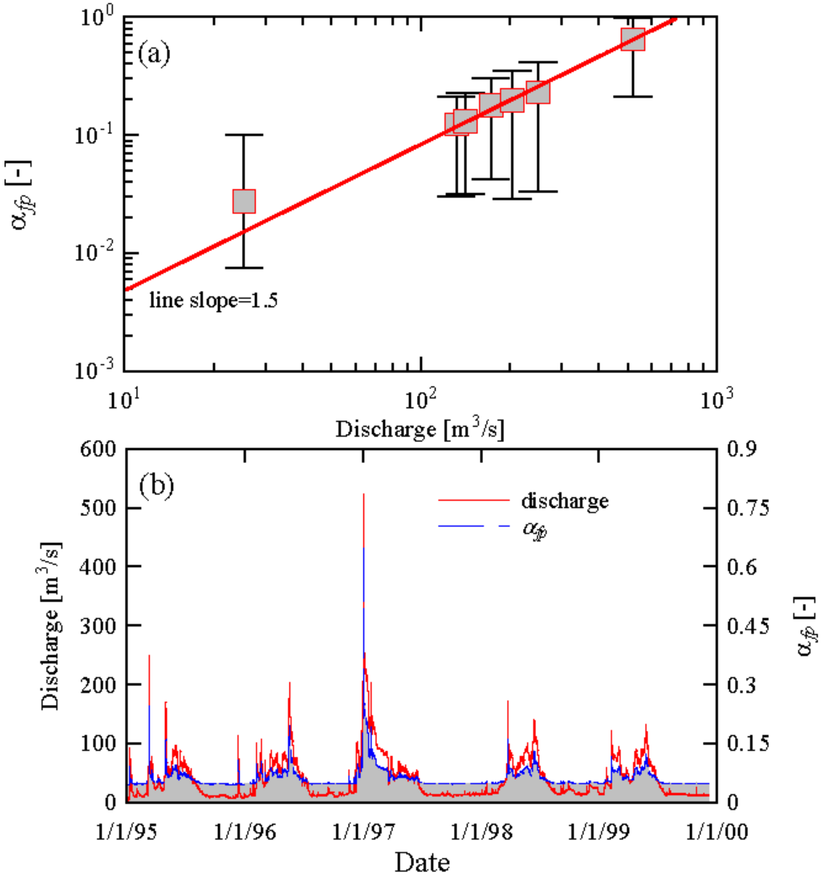

Figure 8. (a) The proportion of total flow that routed through the floodplains (α_{fp}) vs. inflow discharge. The function of the fitted line is $y = 5.0e - 5x^{1.5}$ ($R^2 = 0.984$); **(b)** the mean value of α_{fp} for McCarran ranch from year 1995 to 2000 based on the applying of the former function in **(a)**.

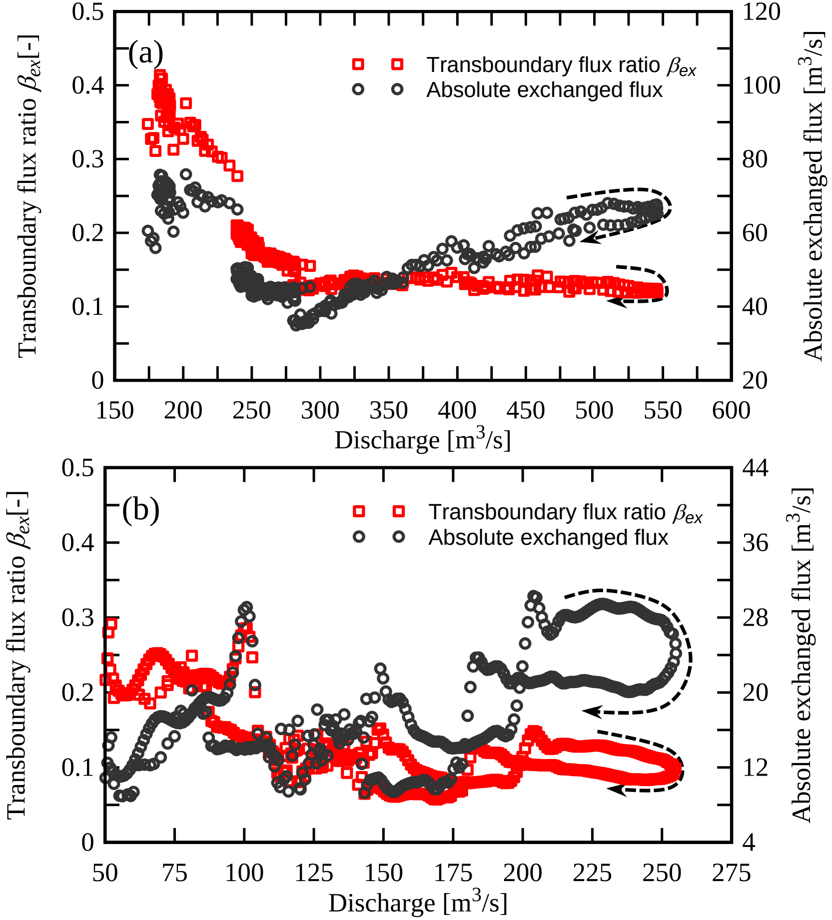

Figure 9. The transboundary flux ratio (or the absolute transboundary flux) vs. river discharge of **(a)** 50 yr flood (case# ⑦) and **(b)** 10 yr flood (case# ⑥).

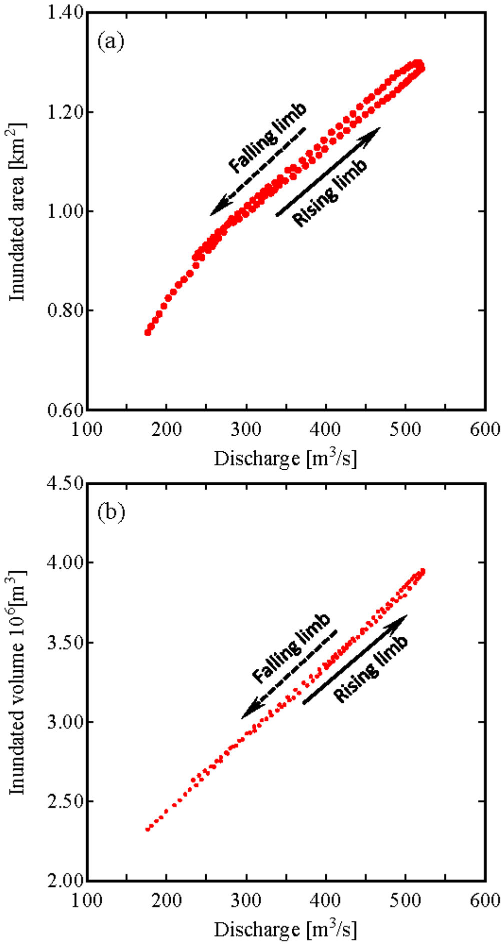

Figure 10. The scatter plots of inundated area vs. discharge **(a)** and inundated volume vs. discharge **(b)** of a sample flood event.